

## General stress-strain model for concrete or masonry response under uniaxial cyclic compression

Lidia La Mendola† and Maurizio Papia‡

*Dipartimento di Ingegneria Strutturale e Geotecnica, Università di Palermo,  
viale delle Scienze 90128-Palermo, Italy*

*(Received April 30, 2002, Accepted August 13, 2002)*

**Abstract.** The paper proposes analytical forms able to represent with very good approximation the constitutive law experimentally deducible by means of uniaxial cyclic compressive tests on material having softening post-peak behaviour in compression and negligible tensile strength. The envelope, unloading and reloading curves characterizing the proposed model adequately approach structural responses corresponding to different levels of nonlinearity and ductility, requiring a not very high number of parameters to be calibrated experimentally. The reliability of the model is shown by comparing the results that it is able to provide with the ones analytically deduced from two reference models (one for concrete, another for masonry) available in the literature, and with experimental results obtained by the authors in the framework of a research in progress.

**Key words:** concrete model; masonry model; uniaxial compression; cyclic loading; constitutive law.

---

### 1. Introduction

Studies on the cyclic behaviour of structural elements made of concrete or masonry are fairly numerous, but they are still encouraged in relation to the high level of detail with which the response of structural systems can be described using advanced computer programs.

When normal stresses mainly occur and the flexural response can be considered to be very slightly influenced by shear stresses, the conventional constitutive law for a generic point can be deduced by means of cyclic uniaxial compression tests, carried out on specimens of standard size, although this approach implies some approximations and, moreover, the size effect on the actual structures cannot be enclosed a priori in the constitutive law obtained in this way.

With reference to concrete, the first experimental investigations aiming at defining reliable constitutive laws go back to the Sixties (Sinha *et al.* 1964, Karsan and Jirsa 1969), but more recently further experimental researches were carried out in order to propose analytical models including the confinement effect (Sheikh and Uzumeri 1980, Ahmad and Shah 1985, Mander *et al.* 1988a, 1988b) or the influence of a different composition of the cementitious matrix (Hsu and Hsu 1994, Nataraja *et al.* 1999, Campione and La Mendola 2001).

With reference to masonry structures, studies on the cyclic response of specimens subjected to

---

† Full Professor of Structural Engineering

‡ Full Professor of Structural Engineering, Head of Department

uniaxial compression are more recent and not so numerous (Abrams *et al.* 1985, Naraine and Sinha 1989a, Subramaniam and Sinha 1995, AlShebani and Sinha 1999, 2000); in the last few years they have proved to be more important in relation to the renewed interest in repair and maintenance of historical and/or monumental buildings in which some regions are rich.

The present study belongs to a theoretical and experimental research addressed precisely to this kind of buildings, but not exclusively, whose bearing structures have been built using local materials from the Mediterranean area. It takes as its starting point the observation that the masonry under consideration experimentally exhibits a stress-strain cyclic law which cannot be described with good approximation by any of the analytical relationships available in the literature, some of them proposed in the works mentioned above. This is due above all to the fact that, a very large variety of components being usable for masonry structures, the constitutive laws which are proposed by each researcher are strictly correlated to the particular features of the masonry tested.

In relation to this difficulty, analytical forms able to represent a large class of constitutive laws in the cyclic field are proposed here; obviously, the general expressions of the normal stress-normal strain relationships discussed later have to be specialized by the calibration of an adequate number of parameters, to be deduced by means of experimental tests. In spite of the aims of the aforementioned research in progress, the proposed model, thanks to its versatility, also allows one to express constitutive laws typical of concrete. For this material the set of  $\sigma - \varepsilon$  curves described below can be assumed to be an alternative model with respect to the very numerous relationships available in the literature, which often, even if expressed in different analytical forms, lead to very similar  $\sigma - \varepsilon$  curves when they are calibrated to represent an actual concrete element.

## 2. Cyclic constitutive law under uniaxial compression

Fig. 1 shows qualitatively the possible cyclic response of a point of a structural element subjected to uniaxial compressive loading, unloading and reloading, assuming the material not to have any tensile strength (masonry or concrete). The stress and strain values are normalized with respect to the compressive strength  $\sigma_{d,o}$  and to the corresponding strain value  $\varepsilon_{d,o}$ , respectively. The ratio between these quantities

$$E_{d,o} = \frac{\sigma_{d,o}}{\varepsilon_{d,o}} \quad (1)$$

is assumed to be the secant modulus characterizing the material.

The figure shows a first loading increasing branch up to the point *A* with coordinates  $\varepsilon_{un}$ ,  $\sigma_{un}$ , at which the unloading phase begins. The latter consists of a first branch in which the normal stress decreases with the corresponding strain, as far as the point *B* with coordinates  $\varepsilon_{pl}$ , 0, followed by a horizontal branch, of equation  $\sigma = 0$ , to the point *C*. Then from this point there originates the reloading path, in which the stress values corresponding to assigned increasing values of strain are measured: the normalized stress remains equal to zero when the normalized strain increases as far as the previous residual value  $\varepsilon_{pl}$ ; then it increases with  $\varepsilon$  so that it again takes on the same pattern as the first loading curve, after the point *F* with coordinates  $\varepsilon_{re}$  and  $\sigma_{re}$  is reached. The point *D* belongs to the “common point curve”, the locus of points closing the hysteresis unloading-reloading cycles. The numbering shown in Fig. 1 denotes the different curves to be expressed analytically for a complete definition of the constitutive model.

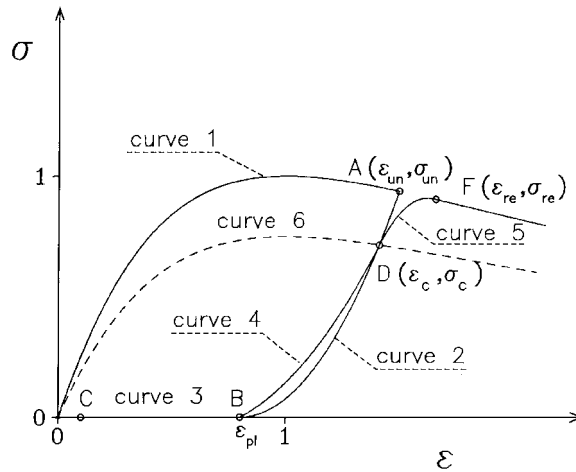


Fig. 1 Typical loading, unloading and reloading paths in normalized plane  $\sigma - \epsilon$

Curve 1 is the envelope curve. Results of many experimental investigations show that this curve is almost the same as the one derived by applying monotonically increasing strains to the specimen, for both concrete and masonry materials. From a physical point of view the shape of the first branch of the (monotonic) envelope curve, up to the maximum stress value, points out the material nonlinearity; a meaningful index of this nonlinearity is the ratio

$$E_i = \frac{E_{d,i}}{E_{d,o}} \quad (2)$$

where  $E_{d,i}$  is the tangent modulus of elasticity at the origin of the curve in the dimensional plane  $\sigma_d - \epsilon_d$ : the higher  $E_i$  is than 1, the more pronounced the material nonlinearity is. The most usual values of  $E_i$  are comprised between 1.5 and 3, for both concrete and masonry materials. In Fig. 1  $E_i$  is the slope of the tangent at the origin of the envelope curve (normalized initial modulus of elasticity). The post-peak branch shows the softening behaviour of the material; it proves to be more or less steep in relation to the lower or higher ductility of the collapse mechanism.

Curve 2 represents the stress pattern during the unloading phase up to the value  $\sigma = 0$ . The nonlinear response of the material implies a residual value of strain, denoted above as  $\epsilon_{pl}$ . In some cases for both concrete (see  $\sigma - \epsilon$  laws in Aoyama and Noguchi 1979) and masonry (La Mendola and Papia 1997) the first stretch of the curve, until the common point curve is reached, is assumed to be vertical, but usually the whole curve  $A - B$  is expressed analytically by a single law, implying calibration of only one parameter. The strain  $\epsilon_{pl}$  is related to the strain  $\epsilon_{un}$  on the basis of experimental results, and this correlation is usually expressed by a quadratic or exponential curve (for concrete see  $\sigma - \epsilon$  laws in Aoyama and Noguchi 1979; for masonry see La Mendola and Papia 1997, Naraine and Sinha 1989b, 1991, AlShebani and Sinha 2000). An alternative approach is proposed in Mander *et al.* (1988b), where the residual strain is substantially calculated by the expression

$$\epsilon_{pl} = \epsilon_{un} - \frac{\sigma_{un}}{E_{s,un}} \quad (3)$$

in which  $E_{s,un}$  is the normalized secant unloading modulus, i.e., the slope of the straight line ideally

linking the points  $A$  and  $B$  in Fig. 1. In this case the experimental results must suggest an appropriate correlation between  $E_{s,un}$  and  $\varepsilon_{un}$ .

The reloading path, from  $B$  to  $F$  in Fig. 1, usually exhibits an analogous shape to that of the unloading curve as far as the point  $D$  (curve 4) located on the common point curve, beyond which it is represented by curve 5, affected by opposite concavity. The calibration of curve 4 must be made carefully for masonry materials, because the hysteresis area delimited by curves 2 and 4 in Fig. 1 is the only dissipative contribution which each point of the structural element can make against external actions. In the case of concrete, since this material is usually utilized with longitudinal steel reinforcement having high dissipative capacity, the reloading curve can be modelled with less precision.

Curve 4 is usually governed by a single parameter to be experimentally calibrated, as for curve 2; curve 5, from  $D$  to  $F$  in Fig. 1, when it is expressed by a distinct law with respect to curve 4, is usually modelled by a quadratic function having the same tangent as the previous curve 4 at the point  $D$ , and final point  $F$  on the envelope curve, whose abscissa  $\varepsilon_{re}$  is correlated to the value  $\varepsilon_{un}$  or  $\varepsilon_{pl}$ . In some models  $\varepsilon_{re}$  is determined by imposing the condition that curve 5 in  $F$  takes on the same tangent as the envelope curve.

Finally, with reference to the common point curve (curve 6 in Fig. 1), it must be observed that its analytical expression is necessary only when curves 4 and 5 are modelled distinctly, because in this case the coordinates of the point  $D$  in Fig. 1 are boundary conditions for both curves and have to be assumed to be known. Otherwise the common point curve is ideally obtained by linking the points at which the reloading curve intercepts the previous unloading curve, without these points necessarily belonging to a curve analytically identified in advance. In the case of masonry materials the common point curve is appreciably distinct from the envelope curve, in particular in the post-peak branch; a systematic study on its pattern is presented in Naraine and Shina (1991). In the case of concrete, envelope and common point curves are fairly close the one to another, so that in some cases they are assumed to be coincident (see  $\sigma - \varepsilon$  laws in Aoyama and Noguchi 1979).

### 3. Analytical and experimental reference data

In order to verify the reliability of the  $\sigma - \varepsilon$  model which will be proposed below, in this section two analytical models (one for concrete and one for masonry) available in the literature are considered, and the analytical expressions on which they are based are briefly commented on. Moreover, data acquired by the direct experimentation related to the research in progress on a particular kind of masonry are described and utilized to validate the model.

#### 3.1 Constitutive reference law for concrete

Systematic experimental investigation on confined concrete specimens (Mander *et al.* 1988a) has made the cyclic model proposed by Mander *et al.* (1988b) highly reliable. In this model the envelope curve (curve 1 in Fig. 1) depends on a single parameter and is expressed by

$$\sigma = \frac{r\varepsilon}{r-1 + \varepsilon^r} \quad (r > 1) \quad (4)$$

in which  $r$  depends on the degree of confinement and is related to the normalized initial modulus of elasticity (Eq. (2)) by

$$E_i = \frac{r}{r-1} \quad (5)$$

Curve 1 tends asymptotically to zero for any value of  $r$ . Low values of  $r$  imply greater values of  $E_i$  (with increasing nonlinearity) and a post-peak branch with a reduced slope, revealing a ductile collapse mechanism.

The unloading curve (curve 2 in Fig. 1) is also governed by a single parameter, and is expressed by

$$\sigma = \sigma_{un} \left( 1 - \frac{r_{un} \bar{\varepsilon}}{r_{un} - 1 + \bar{\varepsilon}^{-r_{un}}} \right) \quad \text{with } r_{un} > 1 \quad \text{and} \quad \bar{\varepsilon} = \frac{\varepsilon - \varepsilon_{un}}{\varepsilon_{pl} - \varepsilon_{un}} \quad (6)$$

The residual strain  $\varepsilon_{pl}$  is related to the strain  $\varepsilon_{un}$  at which unloading begins by Eq. (3), where

$$E_{s,un} = \frac{\sigma_{un} + \varepsilon_a E_i}{\varepsilon_{un} + \varepsilon_a} \quad \text{with} \quad \varepsilon_a = \begin{cases} \frac{1}{1 + \varepsilon_{un}} \sqrt{\varepsilon_{un}} & \text{for } \varepsilon_{un} \leq 2.87 \\ 0.09 \varepsilon_{un}^{3/2} & \text{for } \varepsilon_{un} > 2.87 \end{cases} \quad (7)$$

Eq. (7) in the plane  $E_{s,un} - \varepsilon_{un}$  is a curve starting from the maximum value  $E_{s,un} = E_i$  for  $\varepsilon_{un} = 0$ ; then it decreases rapidly with increases in  $\varepsilon_{un}$ , and for  $\varepsilon_{un} > 3$  exhibits a sub-horizontal pattern, which extends to a large field of values of  $\varepsilon_{un}$ , in which  $E_{s,un} \cong 0.2E_i$  for any value of  $r$ , although analytically it is affected by a minimum value in the range  $4 \leq \varepsilon_{un} \leq 5$ , depending on the value of  $r$ . This sub-horizontal branch exhausts the field of physically admissible values of  $E_{s,un}$ , even if very high ductile behaviour of material is considered.

The parameter  $r_{un}$  which appears in Eq. (6) is linked to the tangent at the origin of the unloading curve (point A in Fig. 1) by the expression

$$\tan \gamma_{un} = E_{s,un} \frac{r_{un}}{r_{un} - 1} \quad (8)$$

this value of the tangent being correlated to the coordinates of the point A on the basis of experimental results. For any value of  $r_{un}$  the unloading curve of Eq. (6) for  $\varepsilon = \varepsilon_{pl}$ , i.e., at the point B in Fig. 1, exhibits a horizontal tangent.

The reloading path consists of two distinct branches (curves 4 and 5 in Fig. 1): the first is expressed by a linear law from the generic point P of curve 2 at which reloading begins (or from the point B in Fig. 1) to the point with coordinates  $\varepsilon_{un}$ ,  $\sigma'_{re}$ , where

$$\sigma'_{re} = 0.92 \sigma_{un} + 0.08 \sigma_{pl} \quad (9)$$

and  $\sigma_{pl}$  is the stress value corresponding to the aforementioned point P ( $\sigma_{pl} = 0$  if reloading originates from the point B); the second branch is a parabolic curve connecting the previous linear branch with the point F (in Fig. 1) on the envelope curve, without discontinuity in the initial and final tangents.

### 3.2 Constitutive reference law for masonry

The constitutive law considered here was proposed in AlShebani and Sinha (2000) on the basis of the results of experimental tests on sand plast brick masonry panels, but it is also able to approach the experimental response of the clay brick masonry panels considered in Subramaniam and Sinha

(1995). The calibration of the parameters characterizing the model is only considered here for the case of loading orthogonal to the mortar bed joints.

The envelope curve is expressed by the law

$$\sigma = \varepsilon e^{(1-\varepsilon)} \quad (10)$$

and exhibits a high level of nonlinearity in the increasing branch ( $E_i = e \cong 2.718$ ) and a brittle collapse mechanism, because the post-peak branch of the curve proves to be fairly steep. In agreement with the latter observation the experimental results presented in the aforementioned papers involve maximum normalized strain values close to 1.5.

The unloading curve (curve 2 in Fig. 1) is modelled by the expression

$$\sigma = C_{un} \sigma_{un} \bar{\varepsilon}^{-n_{un}} \quad \text{with} \quad \bar{\varepsilon} = \frac{\varepsilon - \varepsilon_{pl}}{\varepsilon_{un} - \varepsilon_{pl}} \quad (11)$$

where the following parameter calibrations are proposed:

$$C_{un} = 0.98 \quad \varepsilon_{pl} = 0.47 \varepsilon_{un}^{1.2} \quad n_{un} = 2 + 1.5 \sqrt{\varepsilon_{pl}} \quad (12)$$

The previous expressions allow one to relate the normalized unloading secant modulus to the strain at which unloading begins as follows:

$$E_{s,un} = \frac{e^{(1-\varepsilon_{un})}}{1 - 0.47 \varepsilon_{un}^{0.2}} \quad (13)$$

In the plane  $E_{s,un} - \varepsilon_{un}$  the curve expressed by Eq. (13) exhibits an initial pattern rapidly increasing from  $E_{s,un} = E_i$  for  $\varepsilon_{un} = 0$ , to the value  $E_{s,un} = 1.29 E_i$  for  $\varepsilon_{un} = 0.079$ . This increasing branch is followed by a fairly steep decreasing branch, reducing the value of  $E_{s,un}$  to about one-third of the maximum value when  $\varepsilon_{un} = 1.5$ . Beyond this value of  $\varepsilon_{un}$ , as was observed above, the curve begins to become not physically meaningful; however, analytically it tends asymptotically to zero for  $\varepsilon_{un} \rightarrow \infty$ .

The unloading curve expressed by Eq. (11), considering the presence of the coefficient  $C_{un}$ , actually follows a brief vertical stretch up to the point of coordinates  $(\varepsilon_{un}, 0.98 \sigma_{un})$ ; at this point it is affected by the initial tangent correlated to the exponent  $n_{un}$  (i.e., to  $\varepsilon_{un}$  on the basis of Eqs. (12)) by the expression

$$\tan \gamma_{un} = C_{un} n_{un} E_{s,un} \quad (14)$$

As for the concrete model, this curve exhibits a horizontal tangent at the final point for any value of  $n_{un}$ .

The reloading path, from  $B$  to  $F$  in Fig. 1, is expressed by a single curve:

$$\sigma = \sigma_{re} \bar{\varepsilon}^{-n_{re}} e^{(1-\bar{\varepsilon}^{-n_{re}})} \quad \text{with} \quad \bar{\varepsilon} = \frac{\varepsilon - \varepsilon_{pl}}{\varepsilon_{re} - \varepsilon_{pl}} \quad (15)$$

in which

$$n_{re} = 1.5 + \sqrt{\varepsilon_{pl}} \quad \varepsilon_{re} = \varepsilon_{un} + \delta \varepsilon \quad (16)$$

The parameter  $n_{re}$  governs the shape of the reloading curve, influencing, in particular, the position

of the point at which it changes its concavity. The quantity  $\delta\varepsilon$  is defined as a function of the strains  $\varepsilon_{un}$ ,  $\varepsilon_{pl}$  by means of a correlation calibrated experimentally. Whatever the value of  $n_{re}$ , the curve in Eq. (15) exhibits horizontal tangents at the initial and final points.

### 3.3 Results of experimental tests

The experimental investigation in progress concerns masonry panels, made of calcarenite ashlars connected by mortar joints, subjected to uniaxial monotonic or cyclic compressive actions under controlled displacement.

Calcarenite is a kind of sandstone extracted from superficial quarries. Prismatic and cylindrical specimens of the specific material used to built the masonry panels exhibit a mean compressive strength value of 7.0 MPa and an initial modulus of elasticity about of 12000 MPa. The behaviour in compression is quite linear up to values of stress close to the compressive strength, while the collapse mechanism is very brittle, so that a meaningful post-peak branch in the stress-strain curve cannot be experimentally observed. The mortar is composed by cement, hydraulic lime and calcareous sand, with proportions 1:1:5 by volume. Compression tests on cubic specimens provide a mean strength value of 5.9 MPa and an initial modulus of elasticity of 1505 MPa. The mortar exhibits ductile behaviour up to collapse, with residual strength of about 50% of the compressive strength  $\sigma_{d,o}$  for ultimate strain values 6 to 8 times  $\varepsilon_{d,o}$ .

The masonry panels constructed using these materials consist of one prismatic block of calcarenite ( $360 \times 165 \times 204$  mm) on which two half blocks linked by a vertical mortar joint and a further whole block are placed by interposition of mortar bed joints having a thickness of about 10 mm (Fig. 2). The average strain values during the compression tests are measured on a gauge length of



Fig. 2 Masonry specimen and loading arrangement      Fig. 3 Specimen of greater size and loading arrangement

310 mm by using digimatic indicators, allowing digital and electrical acquisition of data with a reading accuracy of 0.001 mm and symmetrically located with respect to the half height of the panel. The  $\sigma_d - \varepsilon_d$  laws derived by means of these tests are confirmed by similar tests on larger panels, in which linear variable displacement transducers with the same reading accuracy are used on the same gauge length (Fig. 3).

The masonry tested is affected by appreciable strength in compression and high ductility. The cracking mechanism is characterized by initial vertical cracks which become progressively numerous and spread, involving a large part of the specimen (Fig. 4). This mechanism, due to the mutual interactions between the masonry components, neutralizes the brittle behaviour of the calcarenite ashlar, allowing ultimate strain values 5 to 6 times the one corresponding to the strength value. When cyclic loading is applied, cracking propagation becomes more progressive, further attenuating the effects of localized breaking producing some irregularities in the softening branch of the stress-strain curve under monotonic loading. Because of this, the analytical model of the constitutive law better fits the experimental results deduced by means of cyclic tests.

The experimental results considered in this paper refer to four monotonic compression and two cyclic compression tests. The number of tests is not sufficient for a definite calibration of the curves in Fig. 1, but it appears to be adequate to show that the pattern of these curves cannot be analytically described by means of available expressions like the ones commented on above. Considering the constitutive reference law described in the previous sub-section, this circumstance can be justified by the fact that the bricks units utilized by AlShebani and Sinha in their investigation, besides the very different geometry, exhibited a compressive strength of 23.4 MPa, while the compressive cube strength of the mortar was 10.2 MPa, and these values are more than three times and not much less



Fig. 4 Cracking picture and failure mode of specimen

than twice the ones of the corresponding components utilized here (7.0 and 5.9 MPa, respectively). The following sections show the ability of the proposed model to approach with good approximation the compressive response of masonry made of so different materials.

#### 4. Proposed model

##### 4.1 Envelope curve

The envelope curve is modelled by using the analytical form proposed by Sargin (1971) for concrete:

$$\sigma = \frac{A\varepsilon + (D-1)\varepsilon^2}{1 + (A-2)\varepsilon + D\varepsilon^2} \quad (17)$$

The curve is governed by two parameters,  $A$  and  $D$ , whose range of definition and influence on the shape of the curve are deduced from the following comments consequent to the analytical study of Eq. (17): - in the limit case  $A = 1, D = 0$ , Eq. (17) expresses the normalized linear law  $\sigma = \varepsilon$ ; - in the normalized plane  $\sigma - \varepsilon$  the parameter  $A$  is the tangent at the origin of the curve; therefore,  $A = E_i$  with  $E_i$  expressed by Eq. (2); - for  $\varepsilon = 1$   $\sigma$  takes its maximum value ( $\sigma = 1$ ); moreover, the  $\sigma - \varepsilon$  curve must not change its concavity in the range  $0 \leq \varepsilon \leq 1$ ; these two conditions define the field of values of the parameters  $A$  and  $D$  making Eq. (17) physically admissible (excluding the limit case of linear law):

$$1 - A < D \leq (A - 1)^2 \quad \text{with} \quad A = E_i > 1 \quad (18)$$

- the post-peak branch of the  $\sigma - \varepsilon$  curve intersects the strain reference axis for  $\varepsilon > 0$  only if  $D < 1$ , because in this case  $\sigma = 0$  for  $\varepsilon = \varepsilon_{int} = A/(1 - D)$ ; - in relation to the values of the parameters  $A$  and  $D$ , Eq. (17) can be affected by singularities for one or two distinct values of  $\varepsilon$ ; it can be demonstrated that this occurrence is not physically meaningful because it may occur only for  $\varepsilon < 0$  or  $\varepsilon > \varepsilon_{int}$  (for  $D < 1$ ).

The parameters  $A$  and  $D$  allow one to model almost independently the ascending and the post-peak branches of the envelope curve, respectively. Higher values of  $A = E_i$  give greater nonlinearity to the constitutive law, in the sense defined above; higher values of  $D$  represent more ductile behaviour up to collapse. The efficiency of the law assumed can be shown considering the reference models and the experimental data presented in the previous sections. With reference to the concrete model, Eq. (4) is utilized to represent material under two different conditions of confinement, corresponding to the values  $r = 2$  and  $r = 1.5$ , respectively (i.e.,  $E_i = 2$  and  $E_i = 3$  from Eq. (5)). In the first case, setting  $A = 2$  and  $D = 1$ , Eq. (17) becomes identical to Eq. (4); in the second case a very good approximation of the results given by Eq. (4) is obtained by setting  $A = 3$  and  $D = 1.6$  in Eq. (17) (see Fig. 5). Obviously, for a generalized use of Eq. (17) the parameters  $A$  and  $D$  should be related to the confinement parameter  $r$ , but this possible development of investigation lies outside the aims of this work.

With reference to masonry structures, a first remark concerns the fact that Eq. (17), for  $A = 2$  and  $D = 0$ , reproduces the parabolic law proposed by Powell and Hodgkinson (1976) for a particular

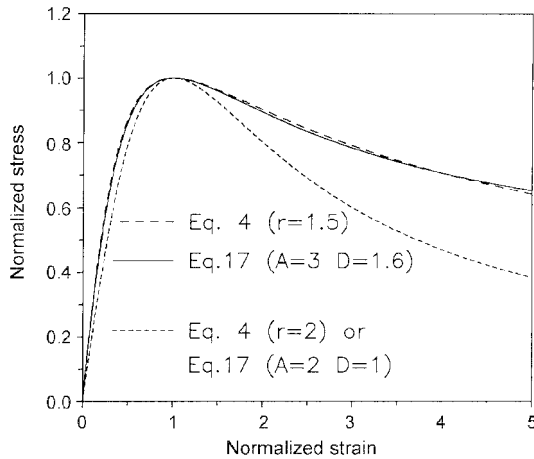


Fig. 5 Reliability of envelope curve adopted with respect to concrete reference model

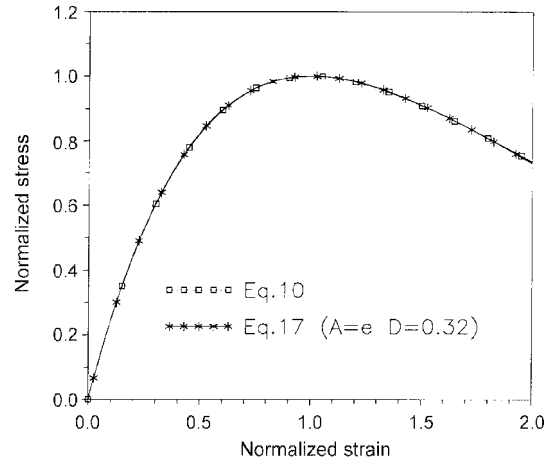


Fig. 6 Reliability of envelope curve adopted with respect to masonry reference model

kind of brick masonry. On the other hand, Fig. 6 shows that Eq. (17), setting  $A = e \cong 2.718$  and  $D = 0.32$ , expresses a curve almost coincident with the one expressed by Eq. (10), which is assumed to be the reference curve in this paper.

Finally, with reference to the experimental data commented on in the previous section, Fig. 7 shows the results referring to the four tests carried out under monotonic loading and their analytical approximation obtained by making Eq. (17) dimensional with  $\sigma_{d,o} = 4.0$  MPa for  $\varepsilon_{d,o} = 0.0013$  and setting  $A = 2.8$  and  $D = 1.2$ . In spite of some scattering of the experimental data, related to the nature of the material, the proposed (monotonic) envelope curve appears to be adequate to express the mean response of the masonry considered.

Concluding this sub-section, some information is given concerning the possible use of the chosen envelope (monotonic) curve for high strength and fibre reinforced concrete, in relation to the recent spread of these materials.

The  $\sigma_d - \varepsilon_d$  constitutive law for unconfined high strength concrete in compression exhibits a quasi-linear ascending branch up to the strength value and a very steep post-peak branch, which is very difficult to obtain experimentally, due to brittle failure mechanism. This law can be simplified to a triangular shape, as in Ali and White (1997). Eq. (17) lends itself to representing this kind of curve in the normalized plane  $\sigma - \varepsilon$ , by assuming a value of the parameter  $A$  not much higher than 1 and the parameter  $D$  very close to the minimum value defining the field in Eq. (18). By way of example Fig. 8 shows some curves obtained by Eq. (17) with  $A = 1.3$ .

The possible use of Eq. (17) for the envelope (monotonic)  $\sigma - \varepsilon$  curve for confined high strength concrete and fibre reinforced concrete has been shown by other authors. For confined high strength concrete this equation is suggested by Watanabe (1997) on the basis of a previous research carried out by Sun and Sakino (1993). With reference to fibre reinforced concrete, Zingone *et al.* (1996) and Nataraja *et al.* (1999) show that the normalized constitutive law in compression derived from cylindrical concrete specimens, reinforced by carbon fibres and steel fibres respectively, can be expressed by Eq. (4), by correlating the parameter  $r$  (denoted as  $\beta$  in their works) to the content and the aspect ratio (length to equivalent diameter ratio) of the fibres. Considering the ability of Eq. (17) to

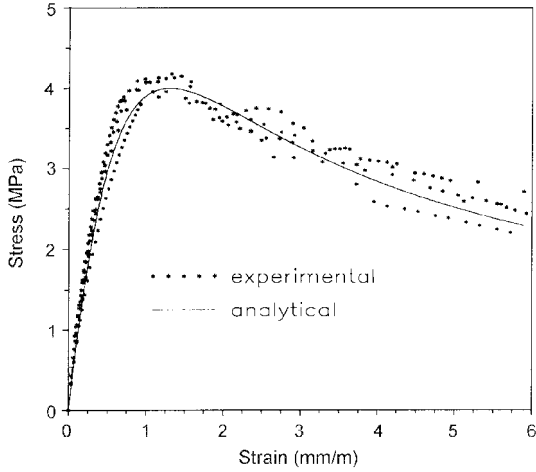


Fig. 7 Experimental and analytical results for monotonically increasing strains

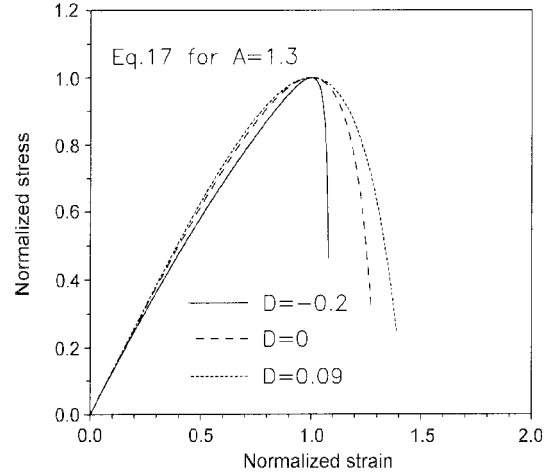


Fig. 8 Shapes of envelope curves with quasi-linear ascending and very steep descending branches

approximate Eq. (4), shown in Fig. 5 for different values of  $r$ , it may thus be inferred that the envelope (monotonic) curve chosen for the present model can be utilized also for fibre reinforced concrete.

#### 4.2 Expressions of residual strain

The proposed approach is based on the use of Eq. (3), because the pursuit of a correlation between  $E_{s,un}$  and  $\epsilon_{un}$  can be founded on physically meaningful considerations on the material properties. This choice justifies the comments made for Eqs. (7) and (13), not essential to presenting the models assumed to be of reference. The two different patterns of the function  $E_{s,un} - \epsilon_{un}$  pointed out for concrete and masonry, respectively, can both be represented by the analytical form

$$E_{s,un} = E_i(a + b e^{-\alpha \epsilon_{un}^\beta}) \quad (19)$$

in which the parameters  $a$  and  $b$  have to be specialized in relation to the ductility expected for the material and to the initial (or quasi-initial) value of  $E_{s,un}$ , corresponding to unloading-reloading cycles in a field of very low strains ( $\epsilon_{un} \rightarrow 0$ ).

For brittle materials, reasonably setting  $E_{s,un} = 0$  for  $\epsilon_{un} \rightarrow \infty$ , one can set  $a = 0$ ; by contrast, for ductile materials  $a$  must be calibrated carrying out one or two unloading-reloading cycles for values of  $\epsilon_{un}$  close to the ultimate value. On the other hand, the sum  $a + b$  must be set to be equal to 1 when the initial value of  $E_{s,un}$  can be assumed to be equal to  $E_i$ , as in the case of concrete, while it must be assumed to be greater than 1 and calibrated experimentally when the initial (or quasi-initial) normalized secant unloading modulus proves to be greater than  $E_i$ , as for masonry.

On the basis of what has just been said, considering the comments made for Eq. (7) concerning the physically admissible values of  $E_{s,un}$ , in the case of concrete Eq. (19) can be written as

$$E_{s,un} = E_i(0.2 + 0.8 e^{-\alpha \epsilon_{un}^\beta}) \quad (20)$$

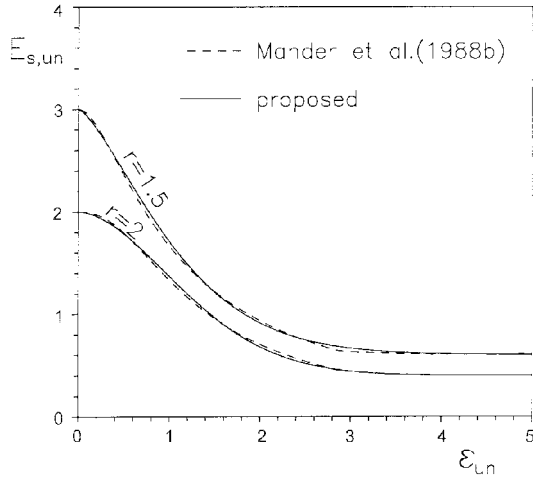


Fig. 9 Comparison of  $E_{s,un} - \epsilon_{un}$  analytical curves for concrete

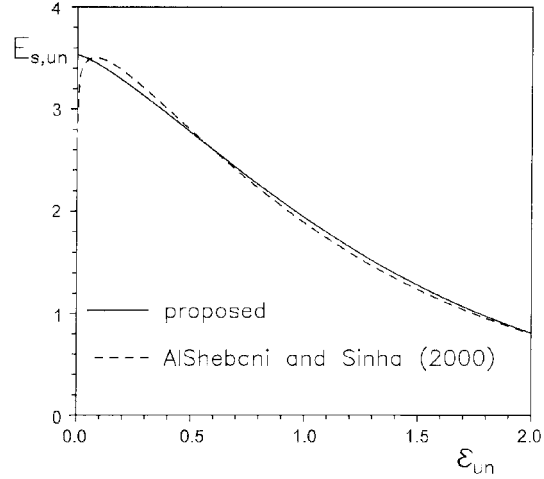


Fig. 10 Comparison of  $E_{s,un} - \epsilon_{un}$  analytical curves for masonry

where the parameters  $\alpha$  and  $\beta$  should be correlated to the value of  $E_i$ , i.e., of  $r$ , as for  $A$  and  $D$  in Eq. (17). Fig. 9 shows the high precision with which this expression approaches Eq. (7) for the values of  $r=2$  and  $r=1.5$  considered in the previous section. The case  $r=2$  is reproduced by using Eq. (20) with  $\alpha=0.50$  and  $\beta=1.80$ ; for  $r=1.5$  the calibrations of the parameters  $\alpha$  and  $\beta$  leads to the values 0.78 and 1.34, respectively.

With regard to the masonry material considered in AlShebani and Sinha (2000), because of brittle behaviour in the post-peak response, one can set  $a=0$  in Eq. (19); moreover, remembering the maximum quasi-initial value of  $E_{s,un}$  stressed commenting on Eq. (13), Eq. (19) can be written in the form

$$E_{s,un} = 1.3E_i e^{-\alpha\epsilon_{un}^\beta} \tag{21}$$

Fig. 10 shows the good level of approximation with which this expression approaches Eq. (13), by assuming  $\alpha=0.60$  and  $\beta=1.30$ .

With reference to the results acquired by direct experimentation, the calibration of the parameters specializing Eq. (19) is made considering for each unloading-reloading cycle the ratio  $E_{s,un} = \sigma_{un}/(\epsilon_{un} - \epsilon_{pl})$ . The values deduced from cycles starting from high values of  $\epsilon_{un}$  (for both cyclic tests) lead to the value  $a=0.3$ ; the ones deduced for very small values of  $\epsilon_{un}$  allow one to assume the initial value of  $E_{s,un}$  equal to  $1.1 E_i$ , and consequently  $b = 1.1 - 0.3 = 0.8$  in Eq. (19). Finally, the values of  $E_{s,un}$  deduced from all the other cycles, executed starting from intermediate values of  $\epsilon_{un}$ , lead for  $\alpha$  and  $\beta$  to the values 0.98 and 1, respectively. Therefore, for the masonry considered Eq. (19) becomes

$$E_{s,un} = E_i(0.3 + 0.8e^{-0.98\epsilon_{un}}) \tag{22}$$

which approaches the experimental results, as shown in Fig. 11.

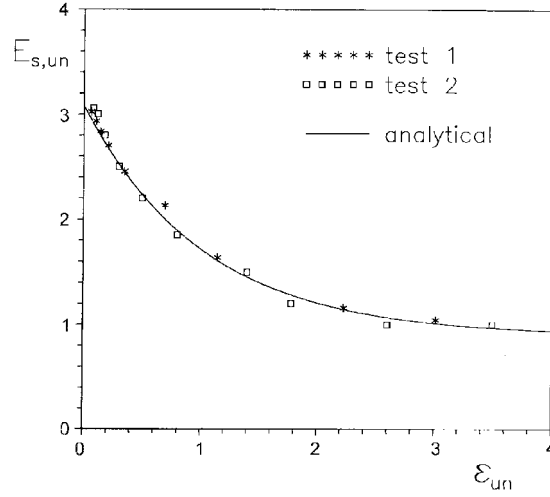


Fig. 11 Comparison between analytical and experimental values of normalized unloading secant modulus

### 4.3 Unloading and reloading curves

The unloading and reloading curves are modelled by a single analytical form to be suitably specialized. Its expression is

$$\bar{\sigma} = \bar{\varepsilon} k_j^{(1 - \bar{\varepsilon}^{m_j})} \quad j = \begin{cases} un & \text{for curve 2 in Fig. 1} \\ re1 & \text{for curve 4 in Fig. 1} \\ re2 & \text{for curve 5 in Fig. 1} \end{cases} \quad (23)$$

with

$$\bar{\sigma} = \frac{\sigma - \sigma_i}{\sigma_f - \sigma_i} \quad \text{and} \quad \bar{\varepsilon} = \frac{\varepsilon - \varepsilon_i}{\varepsilon_f - \varepsilon_i} \quad (24)$$

The subscriptions ( )<sub>i</sub> and ( )<sub>f</sub> refer to the initial and final points of each curve,  $P_i(\varepsilon_i, \sigma_i)$  and  $P_f(\varepsilon_f, \sigma_f)$ , identified by the condition  $\varepsilon_i < \varepsilon_f$ . For each of the three curves, denoted as curves 2, 4 and 5 in Fig. 1,  $k_j$  and  $m_j$  are parameters governing the slopes of the tangents at these points.

For the unloading curve, considering the notation in Fig. 1, one must set  $P_i(\varepsilon_i, \sigma_i) \equiv B(\varepsilon_{pl}, 0)$  and  $P_f(\varepsilon_f, \sigma_f) \equiv A(\varepsilon_{un}, \sigma_{un})$ . Therefore, Eq. (23) is applied with

$$\bar{\sigma} = \frac{\sigma}{\sigma_{un}} \quad \bar{\varepsilon} = \frac{\varepsilon - \varepsilon_{pl}}{\varepsilon_{un} - \varepsilon_{pl}} \quad k_j, m_j = k_{un}, m_{un} \quad (\text{to be calibrated}) \quad (25)$$

Denoting as  $\tan \gamma'_{un}$  the tangent to the curve 2 at the point B, the parameter  $k_{un}$  is calibrated considering that for this curve Eq. (23) gives

$$\tan \gamma'_{un} = k_{un} E_{s,un} \quad (26)$$

Since  $E_{s,un}$  is the slope of the straight line ideally joining the points A and B, the shape of curve 2 shown in Fig. 1 implies the condition  $0 \leq k_{un} \leq 1$ . On the other hand, it may easily be shown that

the slope of the tangent to the curve at the point  $A$  at which the unloading phase begins, already denoted as  $\tan \gamma_{un}$ , by using Eqs. (23), (24) and (25), proves to be

$$\tan \gamma_{un} = (1 - m_{un} \ln k_{un}) E_{s,un} \quad (27)$$

in which  $m_{un}$  must take on a value  $m_{un} > 0$  on the basis of the field of possible values of  $k_{un}$  stressed above.

Both tangents can be calibrated independently of one another, by using first Eq. (26) to calibrate  $k_{un}$  in relation to the measured values of the ratio  $\tan \gamma'_{un} / E_{s,un}$ , and then Eq. (27) once the ratio  $\tan \gamma_{un} / E_{s,un}$  is experimentally evaluated.

All the possible unloading curves expressed by Eq. (23), specialized as was shown above, are comprised between two limit configurations: the first, for  $k_{un} = 1$ , is an unloading linear law from  $A$  to  $B$  for any value of  $m_{un}$ ; the second, for  $k_{un} \rightarrow 0$  and high value of  $m_{un}$ , is a curve having an almost vertical tangent at the point at which unloading begins (point  $A$  in Fig. 1) and a horizontal tangent at the point  $B$ , where the stress takes on zero value. The considerations above allow one to foresee the possibility that any unloading law can be represented with very good precision by suitable calibration of the parameters  $k_{un}$  and  $m_{un}$ .

The analytical expression of the reloading curve 4 in Fig. 1 implies knowledge of the coordinates of the final point  $D(\varepsilon_c, \sigma_c)$ , to be obtained by the intersection of the previous unloading curve with the common point curve which will be described in the next section. The initial point is assumed here to be the point  $B(\varepsilon_{pl}, 0)$ , supposing a previous complete unloading path; however, a reloading originating from any point of curve 2 can also be considered, by suitably correlating the slopes of the tangents to this curve at this initial point (whose coordinates have to be assumed to be known) and at the final point  $D$ .

For the case considered here (curve 4 from  $B$  to  $D$  in Fig. 1) Eq. (23) has to be utilized setting

$$\bar{\sigma} = \frac{\sigma}{\sigma_c} \quad \bar{\varepsilon} = \frac{\varepsilon - \varepsilon_{pl}}{\varepsilon_c - \varepsilon_{pl}} \quad k_j, m_j = k_{re1}, m_{re1} \quad (\text{to be calibrated}) \quad (28)$$

The role of the parameters  $k_{re1}$  and  $m_{re1}$  is the same as that of  $k_{un}$  and  $m_{un}$  for the unloading curve. Therefore, denoting as  $\tan \gamma'_{re1}$  and  $\tan \gamma_c$  the tangents at the initial and final points of the curve (points  $B$  and  $D$  in Fig. 1, respectively) and as

$$E_{s,re1} = \frac{\sigma_c}{\varepsilon_c - \varepsilon_{pl}} \quad (29)$$

the slope of the straight line ideally joining these points, one obtains

$$\tan \gamma'_{re1} = k_{re1} E_{s,re1} \quad (30)$$

$$\tan \gamma_c = (1 - m_{re1} \ln k_{re1}) E_{s,re1} \quad (31)$$

In this case too  $0 \leq k_{re1} \leq 1$  and  $m_{re1} > 0$  must be assumed, but the field of possible values of these parameters must now take the previous calibration of the unloading curve into account. In this connection, it must be observed that the reloading curve proves to be physically meaningful if  $\tan \gamma'_{re1} \geq \tan \gamma'_{un}$  and  $\tan \gamma_c \leq (d\sigma/d\varepsilon)_{\varepsilon=\varepsilon_c}$ , where the derivative refers to the function  $\sigma(\varepsilon)$  expressed by Eq. (23) specialized for the unloading curve.

The second branch of the reloading path (curve 5 from  $D$  to  $F$  in Fig. 1) is again expressed by using Eq. (23), but setting

$$\bar{\sigma} = \frac{\sigma - \sigma_c}{\sigma_{re} - \sigma_c} \quad \bar{\varepsilon} = \frac{\varepsilon - \varepsilon_c}{\varepsilon_{re} - \varepsilon_c} \quad k_j, m_j = k_{re2}, m_{re2} \quad (32)$$

The analytical expression of this curve implies knowledge of the coordinates of the final point  $F(\varepsilon_{re}, \sigma_{re})$ , but it does not imply calibration of further parameters, because  $k_{re2}$  and  $m_{re2}$  must be determined by imposing the condition that the curve at the initial point  $D$  is affected by the same tangent as the previous curve 4, and at the final point  $F$  by the same tangent as the envelope curve to which this point belongs.

Consequently the only calibration required concerns the value of  $\varepsilon_{re}$ , which is determined here by using the second of Eqs. (16), in which

$$\delta\varepsilon = c(\varepsilon'_{re} - \varepsilon_{un})^{0.5} \quad (33)$$

where  $\varepsilon'_{re}$  is the abscissa of the point at which the straight line ideally joining the points  $B$  and  $D$  in Fig. 1, with slope  $E_{s, re1}$  expressed by Eq. (29), intersects the envelope curve;  $c$  is a coefficient to be calibrated by experimental data. Once  $\varepsilon_{re}$  is known, Eq. (17) and its derivative for  $\varepsilon = \varepsilon_{re}$  give  $\sigma_{re}$  and  $\gamma_{re}$ , respectively, the latter being the tangent to the envelope curve at the point  $F(\varepsilon_{re}, \sigma_{re})$ .

Then the aforementioned condition of continuity of the tangent at the initial and final points of the curve gives

$$k_{re2} = (1 - m_{re1} \ln k_{re1}) \frac{E_{s, re1}}{E_{s, re2}} \quad (34)$$

$$m_{re2} = \frac{1}{\ln k_{re2}} \left( 1 - \frac{\tan \gamma_{re}}{E_{s, re2}} \right) \quad (35)$$

in which the secant modulus of this reloading curve  $E_{s, re2}$  is expressed by

$$E_{s, re2} = \frac{\sigma_{re} - \sigma_c}{\varepsilon_{re} - \varepsilon_c} \quad (36)$$

It must be observed that the modelling proposed for curve 5 involves the need to verify that this curve, from the point  $D$  to the point  $F$  in Fig. 1, remains below the envelope curve, as experimentally observed. From an analytical point of view, considering the assumptions for the initial and final tangents, this condition implies that the curve does not change its concavity in the whole field of definition  $\varepsilon_c \leq \varepsilon \leq \varepsilon_{re}$ . It can be demonstrated that this is verified if  $\tan \gamma_{re} > 0$ , i.e., if the final point  $F$  belongs to the ascending branch of the envelope curve; otherwise, if  $\tan \gamma_{re} < 0$ , the curve does not admit a flex point if

$$E_{s, re} \geq \tan \gamma_{re} (1 - \ln k_{re2}) \quad (37)$$

Therefore, if Eq. (34) gives  $k_{re2} < e (\cong 2.718)$ , Eq. (37) is certainly verified, because it cannot happen that  $E_{s, re2} < 0$  (see Eq. (36)); if  $k_{re2} > e$  Eq. (37) can imply the need to reduce the value of  $\delta\varepsilon$  provided by Eq. (33) so that the first member of Eq. (37) becomes equal to the second.

#### 4.4 Common point curve

On the basis of what observed above, the proposed model involves an analytical definition of the common point curve. By using the same criterion as proposed in Naraine and Sinha (1991), this

curve can be obtained from the envelope curve equation (Eq. (17)), substituting the variables  $\sigma$  and  $\varepsilon$  appearing in it with the stress and strain variables  $\sigma' = \sigma/c_\sigma$  and  $\varepsilon' = \varepsilon/c_\varepsilon$ , in which  $c_\sigma$ ,  $c_\varepsilon$  are coefficients to be suitably calibrated. This substitution modifies the coordinates of the point corresponding to the maximum value of the function in the normalized plane  $\sigma-\varepsilon$  and, consequently, the shape of the original curve. Considering the analytical form chosen in the proposed model for the envelope curve, a further possibility of better modelling the common point curve to fit experimental results lies in also modifying the parameters  $A$  and  $D$  appearing in Eq. (17), if necessary.

## 5. Reliability of proposed model

The first two following applications show the ability of the proposed model to give very similar normalized constitutive cyclic laws as the models assumed to be of reference for concrete and masonry; the third application shows its efficiency in fitting the experimental results deduced in the framework of the research in progress.

### 5.1 Application 1

For confined concrete with confinement level corresponding to  $r = 1.5$  ( $E_i = 3$ ) according to the model of Mander *et al.* (1988b), four unloading-reloading cycles, starting from the values  $\varepsilon_{un} = 0.75, 1.5, 2.5, 4$ , are considered.

Using the reference model, the envelope curve is expressed by Eq. (4) and the normalized residual strain at each cycle is derived from Eq. (3) with  $E_{s,un}$  expressed by Eq. (7). In agreement with the correlation utilized in this reference model, the slope of the tangent to the unloading curve at the point at which unloading begins is expressed by

$$\tan \gamma_{un} = \frac{\sigma_{un}}{\sigma_{co}} \frac{1}{\sqrt{\varepsilon_{un}}} E_i \quad (38)$$

where  $\sigma_{co}$  is the compressive strength of the unconfined concrete, normalized with respect to that of confined concrete, and the two ratios multiplying  $E_i$  must be assumed to be equal to 1 when they prove to be lower and higher than 1, respectively. For this example  $\sigma_{co}$  is assumed to be equal to 0.5. By using Eq. (38), the parameter  $r_{un}$ , governing the unloading curve of Eq. (6), is deduced from Eq. (8).

The linear law of the reloading branch is defined once the stress  $\sigma'_{re}$  expressed by Eq. (9) (with  $\sigma_{pl} = 0$ ) is known, while the analytical expression of the parabolic curve following this linear branch is determined by imposing the condition that this previous straight line is tangent to the curve at its initial point, and the curve is affected by the same tangent as the envelope curve at the final point belonging to it.

To reproduce the same cycles by using the proposed model, the envelope curve is expressed by Eq. (17) with the same calibration as for the results in Fig. 5, while the normalized unloading secant modulus  $E_{s,un}$  is expressed as for the results in Fig. 9. Once  $\varepsilon_{pl}$  is derived for each cycle from Eq. (3), the parameters characterizing the unloading curves are assumed so that they provide more or less the same tangents at the initial and final points of the curve as in the original reference model. Therefore,  $k_{un}$  is assumed to be  $k_{un} = 10^{-6}$  (for this value Eq. (26) gives  $\tan \gamma'_{un} \cong 0$ ), while  $m_{un}$  is

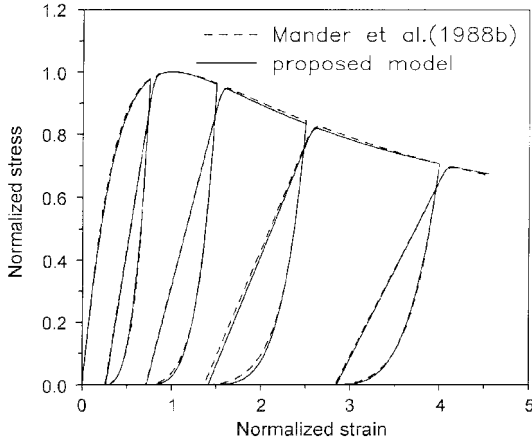


Fig. 12 Reliability of proposed model with respect to concrete reference model

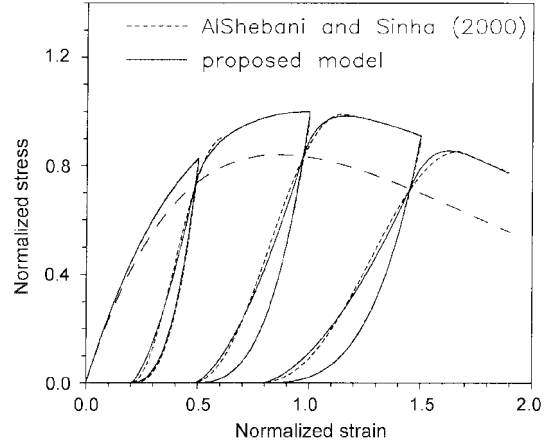


Fig. 13 Reliability of proposed model with respect to masonry reference model

obtained from Eq. (27) where  $\tan\gamma_{um}$  is expressed by Eq. (38).

For the reloading curves the linear branch is governed by the slope  $E_{s,rel}$  deduced from knowledge of the coordinates  $(\epsilon_{um}, 0.98\sigma_{um})$  of the final point; curve 5 is expressed by Eq. (23) specialized by using Eqs. (32), where the only calibration required concerns the value of  $c$  to be introduced in Eq. (33) to calculate  $\delta\epsilon$ . On the basis of the results given by the reference model, for this example it is assumed to be  $c = 0.5$ .

The comparison between the normalized constitutive cyclic laws obtained by using the original and the proposed models is shown in Fig. 12.

### 5.2 Application 2

For the masonry material tested by AlShebani and Sinha (2000) a loading history including three unloading-reloading cycles, starting from  $\epsilon_{um} = 0.5, 1, 1.5$ , is considered.

With reference to the original model, the following expressions have to be utilized: Eq. (10) for the envelope curve; Eqs. (11) and (12) for the unloading curves; Eqs. (15) and (16) for the reloading curves. To calculate the values of  $\epsilon_{re}$  for each cycle, the expression of  $\delta\epsilon$  appearing in the second of Eqs. (16) is calibrated by imposing the condition that the common points, obtained by intersections of each reloading curve with the previous unloading curve, belong to the common point curve defined in Naraine and Sinha (1989a). This curve is expressed by Eq. (10), substituting the stress value at the first member with the ratio  $\sigma' = \sigma/c_\sigma$  and the strain at the second member with the ratio  $\epsilon' = \epsilon/c_\epsilon$ , and assuming  $c_\sigma = 0.84$  and  $c_\epsilon = 0.85c_\sigma + 0.15$ . This condition leads to the correlation

$$\delta\epsilon = 0.085 + 1.936\left(\frac{\epsilon_{pl}}{\epsilon_{un}}\right)^{4.57} \quad (39)$$

The use of the proposed model is based on the previous calibrations of the envelope curve and of the normalized unloading secant modulus (see results in Figs. 6 and 10, respectively). The two parameters governing the unloading curves are calibrated by the same criterion as for Application 1; therefore,  $k_{um}$  is again assumed to be  $k_{um} = 10^{-6}$  ( $\tan\gamma'_{un} \cong 0$  as in the original model), while  $m_{un}$  is

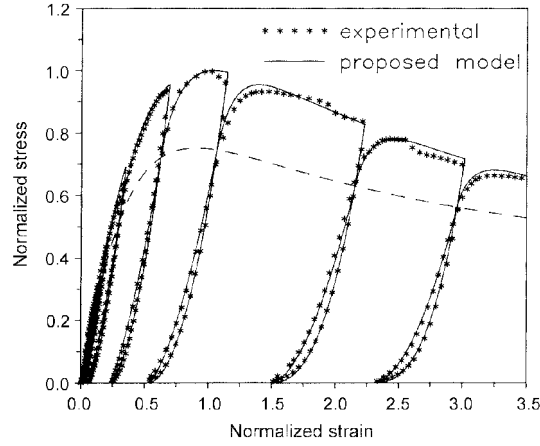


Fig. 14 Ability of proposed model to fit experimental results

obtained by equating the expression at the second member of Eq. (14), in which  $C_{un}$ ,  $n_{un}$  are expressed by means of Eqs. (12), with the expression at the second member of Eq. (27).

For the reloading curves, considering that the common point curve is analytically defined by Eq. (17) specialized for this case ( $A = e$ ,  $D = 0.32$ ) and using the variables  $\sigma' = \sigma/c_\sigma$  and  $\varepsilon' = \varepsilon/c_\varepsilon$  stressed above, one must determine the parameters  $k_{re1}$  and  $m_{re1}$  governing the first reloading branch (curve 4 in Fig. 1), and the coefficient  $c$  making it possible to locate the final point of curve 5 on the envelope curve. The parameter  $k_{re1}$ , appearing in Eq. (30), is assumed to be  $k_{re1} = 10^{-6}$ , considering that  $\tan \gamma'_{re} = 0$  in the original model; the exponent  $m_{re1}$  is correlated to the analogous exponent governing the unloading curve setting  $m_{re1} = 0.28 m_{un}$ ; the coefficient  $c$  appearing in Eq. (33), on the basis of results given by Eq. (39), is assumed to be  $c = 1.1$ .

The good level of precision achievable with the proposed model is shown in Fig. 13.

### 5.3 Application 3

The experimental results utilized for this application refer to one of the two cyclic tests commented on in section 4 (test 1 in Fig. 11); as in the previous applications they are normalized preliminarily with respect to the values  $\sigma_{d,o}$  and  $\varepsilon_{d,o}$ .

The specimen was subjected to nine complete unloading-reloading cycles, the first four in a field of very small strains (to calibrate the initial value of the normalized unloading secant modulus) so that their distinct graph is difficult to get.

The experimental results are analytically approached by the proposed model, by using the following expressions and calibrations of parameters: - the envelope curve is expressed by Eq. (17) setting  $A = 2.8$  and  $D = 1.2$ , as already done for the results in Fig. 7; - the common point curve is expressed by Eq. (17) for  $A = 2.8$ ,  $D = 1.6$ ,  $\sigma' = \sigma/0.75$ ,  $\varepsilon' = \varepsilon/0.9$ ; - for the unloading curves  $E_{s,un}$  is expressed by Eq. (22), as shown in Fig. 11,  $\varepsilon_{pl}$  is calculated by Eq. (3), the pattern of the initial and final tangents to the curves are evaluated by

$$\tan \gamma'_{un} \cong 0 \quad \tan \gamma_{un} = (1 + 1.3 \varepsilon_{pl}^{0.35}) E_{s,un} \quad (40)$$

and consequently  $k_{un}$  is assumed to be  $k_{un} = 10^{-6}$  while  $m_{un}$  is correlated to  $\varepsilon_{pl}$  (i.e., to  $\varepsilon_{un}$ ) by

equating the second member of Eq. (40) with the second member of Eq. (27); - the first curve of the reloading path is analytically defined by assuming  $k_{re1} = k_{un}$  and  $m_{re1} = 0.5m_{un}$ ; - the second curve (curve 5 in Fig. 1) is defined by assuming  $c = 1.4$  in Eq. (33).

The very good level of precision of the modelling adopted is shown in Fig. 14.

The assumption of values very close to zero for the parameters  $k_{un}$  and  $k_{re1}$  in the applications presented here could make it appear advisable to choose for curves 2 and 4 in Fig. 1 analytical forms governed by a single parameter as in the reference models considered. But it must be observed that this possible assumption would imply some meaningful limitations when the reloading curve originates from any point of the previous unloading curve and not from that affected by stress equal to zero, or, more in general, when different materials characteristics (above all as regards masonry materials) are considered.

## 6. Conclusions

An analytical model able to reproduce the constitutive law for concrete or masonry subjected to uniaxial cyclic compression has been proposed. This model defines the stress-strain law in the normalized plane and it allows one to give the results in dimensional form once the compressive strength of the material and the corresponding strain value are known.

The proposed model consists of four analytical laws devoted to representing: (1) the (monotonic) envelope curve; (2) the unloading path from a point belonging to the envelope curve; (3) a first reloading path up to the common point curve; (4) a second reloading path, following the first, up to the final point completing the cycle, belonging to the envelope curve.

The analytical expression of the envelope curve, which is not an original formulation (Sargin 1971), has been chosen on account of its versatility: two parameters, the one having a large field of definition with respect to the other, allow one to model almost independently the increasing branch, depending on the material nonlinearity, and the post-peak softening branch, related to the ductility of the cracking mechanism.

On the other hand, a single analytical form for unloading and reloading curves has been proposed, to be suitably specialized for each curve. The unloading curve and the first curve of the reloading path involve calibration of two parameters each, defining the patterns of the tangents at the initial and final points, which can also be modelled almost independently of one another; instead, the second curve of the reloading path only implies knowledge of the coordinates of the final point of the cycle, located on the envelope curve.

On the basis of what has just been said, the proposed model requires in all calibration of six parameters and two correlations, the first for the residual strain (more precisely for the unloading secant modulus), the second for the strain corresponding to the final point of the cycle, both quantities to be related to the strain at which the unloading path begins. The analytical definition of the common point curve is also necessary.

The modest burden due to a greater number of parameters to be calibrated with respect to other models available in the literature is amply counterbalanced by the versatility of the model. In this connection the applications presented here show the ability of the proposed analytical forms to reproduce results given by reference models for concrete and masonry, and their ability to fit experimental results obtained on masonry tested by the authors in the course of an experimental research in progress.

## References

- Abrams, D., Noland, J. and Atkinson, R. (1985), "Response of clay unit masonry to repeated compressive forces", *Proc. 7th International Brick Masonry Conference*, Melbourne.
- Ahmad, S.M. and Shah, S.P. (1985), "Behavior of hoop confined concrete under high strain rates", *ACI J.*, **82** (5), 195-211.
- Ali, M.A. and White, R.N. (1997), "On extending ACI 318 to high strength concrete", *Proc. First International Conference "High Strength Concrete"*, Kona, Hawaii.
- AlShebani, M.M. and Sinha, S.N. (1999), "Stress-strain characteristics of brick masonry under uniaxial cyclic loading", *J. Struct. Div.*, ASCE, **125**(6), 600-604.
- AlShebani, M.M. and Sinha, S.N. (2000), "Cyclic compressive loading-unloading curves of brick masonry", *Struct. Eng. Mech.*, **9**(4), 375-382.
- Aoyama, H. and Noguchi, H. (1979), "Mechanical properties of concrete under load cycles idealizing seismic actions", *Structural concrete under seismic actions, State of the art reports*, CEB **131**(1), Ed. Scientifiche associate, Roma.
- Campione, G. and La Mendola, L. (2001), "Stress-strain behavior in compression of lightweight fiber reinforced concrete under monotonic and cyclic loads", *Proc. 3rd Conference on Earthquake Resistant Engineering Structures*, Malaga.
- Hsu, L.S. and Hsu, C.T.T. (1994), "Stress-strain behavior of steel-fiber high strength concrete under compression", *ACI Struct. J.*, **91**(4), 448-457.
- Karsan, J.K. and Jirsa, J.O. (1969), "Behaviour of concrete under compressive loadings", *J. Struct. Div.*, ASCE, **95**(ST 12), 2543-2563.
- La Mendola, L. and Papia, M. (1997), "Safety condition of masonry columns subjected to horizontal forces: effects of material nonlinearity and cyclic loading", *Structural Studies, Repairs and Maintenance of Historical Buildings, STREMAH V*, Computational Mechanics Publications, Southampton (U. K.).
- Mander, J.B., Priestley, J.N. and Park, R. (1988a), "Observed stress-strain behavior of confined concrete", *J. Struct. Engrg.*, ASCE, **114**(8), 1827-1849.
- Mander, J.B., Priestley, J.N. and Park, R. (1988b), "Theoretical stress-strain model for confined concrete", *J. Struct. Div.*, ASCE, **114**(8), 1804-1826.
- Naraine, K. and Sinha, S.N. (1989a), "Behavior of brick masonry under cyclic compressive loading", *J. Construction Engrg. and Management*, ASCE, **115**(2), 1432-1445.
- Naraine, K. and Sinha, S.N. (1989b), "Loading and unloading stress-strain curves for brick masonry", *J. Struct. Div.*, ASCE, **115**(10), 2631-2643.
- Naraine, K. and Sinha, S.N. (1991), "Cyclic behavior of brick masonry under biaxial compression", *J. Struct. Engrg.*, ASCE, **117**(5), 1336-1355.
- Nataraja, M.C., Dhang, N. and Gupta, A.P. (1999), "Stress-strain curves for steel-fiber reinforced concrete under compression", *Cement & Concrete Composites*, **21**(5-6), 383-390.
- Powell, B. and Hodgkinson, H.R. (1976), "The determination of stress-strain relationship of brickwork", *Proc. 4th International Brick Masonry Conference*, Bruges.
- Sargin, M. (1971), "Stress-strain relationship for concrete and the analysis of structural concrete sections", *Study 4, Solid Mechanics Division*, University of Waterloo, Waterloo, Ontario.
- Sinha, B.P., Gerstle, K.H. and Tulin, L.G. (1964), "Stress-strain relations for concrete under cyclic loading", *ACI J.*, **61**(2), 195-211.
- Subramaniam, K.V. and Sinha, S.N. (1995), "Analytical model for cyclic compressive behaviour of brick masonry", *ACI Struct. J.*, **92**(3), 288-294.
- Sun, Y.P. and Sakino, K. (1993), "Axial behaviors of confined high strength concrete", *Transactions of the Japan Concrete Institute*, 455-462.
- Watanabe, F. (1997), "Research activities on high strength concrete and its application in Japan", *Proc. First International Conference "High Strength Concrete"*, Kona, Hawaii.
- Zingone, G., La Mendola, L. and Campione, G. (1996), "The ductility of carbon fibre reinforced concrete joints in seismic areas", *Proc. 11th World Conference on Earthquake Engineering*, Acapulco.